RADIATION RESEARCH **164**, 680–687 (2005)
0033-7587/05 $15.00

Noninvasive Quantitative *In Vivo* Mapping and Metabolism of Boronophenylalanine (BPA) by Nuclear Magnetic Resonance (NMR) Spectroscopy and Imaging

Peter Bendel,[a,1] Raanan Margalit,[b] Natalia Koudinova[b] and Yoram Salomon[b]

[a] *Chemical Research Support and* [b] *Biological Regulation Department, The Weizmann Institute of Science, Rehovot 76100, Israel*

Bendel, P., Margalit, R., Koudinova, N. and Salomon, Y. Noninvasive Quantitative *In Vivo* Mapping and Metabolism of Boronophenylalanine (BPA) by Nuclear Magnetic Resonance (NMR) Spectroscopy and Imaging. *Radiat. Res.* 164, 680–687 (2005).

^{10}B-enriched L-*p*-boronophenylalanine (BPA) is one of the compounds used in boron neutron capture therapy (BNCT). In this study, several variations of nuclear magnetic resonance spectroscopy (MRS) and spectroscopic imaging (MRSI) were applied to investigate the uptake, clearance and metabolism of the BPA-fructose complex (BPA-F) in normal mouse kidneys, rat oligodendroglioma xenografts, and rat blood. Localized ^{1}H MRS was capable of following the uptake and clearance of BPA-F in mouse kidneys with temporal resolution of a few minutes, while ^{1}H MRSI was used to image the BPA distribution in the kidney with a spatial resolution of 9 mm^3. The results also revealed significant dissociation of the BPA-F complex to free BPA. This finding was corroborated by ^{1}H and ^{11}B NMR spectroscopy of rat blood samples as well as of tumor samples excised from mice after i.v. injection of BPA-F. This investigation demonstrates the feasibility of using ^{1}H MRS and MRSI to follow the distribution of BPA *in vivo*, using NMR techniques specifically designed to optimize BPA detection. The implementation of such procedures could significantly improve the clinical efficacy of BNCT.

INTRODUCTION

Boron neutron capture therapy (BNCT) requires the administration of ^{10}B-enriched molecules (''BNCT agents''), which are subsequently irradiated with thermal or epithermal neutrons, producing local high-linear energy transfer (LET) radiation that destroys the tumor cells (*1*). For an optimized clinical outcome, it would be desirable to measure and map the boron concentration in blood, tumor and surrounding tissue throughout the treatment, for two main reasons. First, the optimal timing for the neutron irradiation depends on the boron concentration in the tumor, which should be as high as possible, but also on its concentration in blood and surrounding tissue, which should be as low as possible. Second, quantitative knowledge of the local boron concentration is necessary for calculating the radiation dose for treatment planning. Despite its obvious importance, noninvasive online mapping of the boron distribution has not been implemented and applied in clinical practice. Various techniques for determining boron levels in blood and tissue samples (*2, 3*) provided empirical data on uptake and distribution, and models based on these data, rather than real-time measurements in patients during the actual treatment, are used in clinical practice (*4–8*). In the case of L-*p*-boronophenylalanine (BPA), it was also demonstrated that ^{18}F-labeled BPA could be imaged by positron emission tomography (PET), and this was used for determining boron uptake and distribution kinetics in pretreatment ''rehearsal'' studies (*9–11*).

Nuclear magnetic resonance (NMR) is a long-established noninvasive analytical measurement tool that is also commonly applied *in vivo*, mainly in the form of magnetic resonance imaging (MRI) or localized spectroscopy (MRS) (*12–14*). MRI provides images of molecules (usually water) without resolving their signature resonance frequencies (''chemical shifts''), while MRS produces spectra from localized regions (''voxels'') in the specimen. The term spectroscopic imaging (SI) or magnetic resonance spectroscopic imaging (MRSI) is applied for techniques that combine MRI and MRS by simultaneously acquiring spectra from many voxels, which can be used to provide separate images of the different metabolite signals appearing in the spectra. Localized, *in vivo* MRS was applied previously and was shown to be valuable for following the uptake and distribution of drugs in humans. Among other studies, ^{7}Li NMR was used for metabolic studies of lithium administered for treating bipolar disorder (*15*) and ^{19}F NMR for the detection and imaging of different fluorinated drugs (*16–18*).

The most straightforward approach for detecting ^{10}B-enriched molecules is the use of ^{10}B NMR, which was shown by us to be feasible for the imaging of the BNCT agent BSH (*19, 20*). However, for BPA, certain experimental cir-

[1] Address for correspondence: Chemical Research Support MR Center, The Weizmann Institute of Science, 240 Herzel St., Rehovot 76100, Israel; e-mail: Peter.Bendel@weizmann.ac.il.

cumstances favor another approach, namely the detection of the molecule by the signal from some of its hydrogen atoms, using ^{1}H NMR. This suggestion and a demonstration thereof were presented by Zuo *et al.* (*21*), who showed a localized BPA spectrum from a patient's brain, using a clinical scanner and a standard MRS acquisition protocol. Subsequent reports focused on the characterization of the ^{1}H NMR signal from BPA-fructose (BPA-F) for standard MRS protocols in phantom solutions (*22*, *23*). In the present study, ^{1}H detection of BPA was applied to live mice, using improved and optimized protocols for single-voxel MRS as well as MRSI. A more detailed description of the NMR methodology and its validation has been published elsewhere (*24*). ^{1}H and ^{11}B NMR spectroscopy were also applied to rat blood and excised tumor samples to complement and corroborate some of the *in vivo* results.

MATERIALS AND METHODS

BPA-Fructose (BPA-F)

L-*p*-Boronophenylalanine at natural isotopic abundance was purchased from Katchem (Prague, Czech Republic) and used without further purification. Since the solubility of BPA is limited, solutions for administration to animals were prepared by dissolving BPA in the presence of ~15% molar excess of fructose, under continuous adjustment of the pH to basic conditions. The final pH of the injection solution was 8.6, and the final total BPA concentration was 0.26 *M*, partitioned between the BPA-F complex and free BPA. The BPA concentration in the injection solution was determined by high-resolution ^{1}H NMR spectroscopy in which the BPA solution was diluted with a reference solution containing a known concentration (33 m*M*) of glycine in D_2O.

Animal Experiments

All experiments were conducted according to the guidelines of the institutional animal care and use committee of the Weizmann Institute of Science, Rehovot, Israel.

Uptake of boronated compounds in mouse kidneys. Eight-week-old CD1 nude male mice (20–25 g) were anesthetized with a 7:3 N_2O:O_2 mixture containing 0.5–1.5% isoflurane (Medeva, Bethlehem, PA). The mice were positioned inside the horizontal bore of the MRI scanner with an infusion line connected to the tail vein. After initial adjustments and collection of preinjection NMR data, about 1 ml of the BPA/BPA-F solution was infused at a rate of about 17 μl/min using a Gilson® Minipuls3 infusion pump (Villiers-le-Bel, France). The total administered dose corresponded to about 2 g BPA/kg.

Blood clearance experiments. A total of 1.7 ml of the standard (0.26 *M*) BPA-F solution was injected as a single bolus into the tail vein of a ~250 g male Wistar rat. This corresponds to 0.37 g BPA/kg, or 19 mg/kg boron. Peripheral blood samples (~0.5 ml) were collected at different times after BPA-F injection, diluted in water to 2 ml, and examined by ^{1}H and ^{11}B NMR. Before the NMR spectroscopy was performed, the samples were centrifuged and the pellet was removed to achieve sharper lines in the spectra.

Uptake of BPA in tumors. B33 rat oligodendroglioma cells in single cell suspension were implanted subcutaneously (s.c.) into the upper hind legs of CD1 nude mice (2×10^6 cells per mouse). The tumor-bearing mice were injected with 0.4 ml of the BPA-F solution (0.26 *M*) into the tail vein, corresponding to about 0.87 g BPA/kg, or 45 mg boron/kg. Tumors were excised 18 and 42 min after injection. The tumors were weighed, homogenized and transferred to a 10-mm NMR tube in which the volume was increased to 2.5 ml by the addition of saline to be equal to that of a reference solution containing a known total BPA concentration.

NMR Measurements

In vivo experiments. Experiments on live animals were conducted on a Biospec Avance™ system (Bruker Biospin, Ettlingen, Germany) with a 4.7 T 30-cm horizontal bore magnet. For the experiments described here, we used the main actively shielded 20-cm i.d. gradient coil, with a maximal intensity of 100 mT/m and 0.33-ms rise time. The RF probe system included a 7.5-cm resonator for pulse transmission and a 2.5-cm circular receive-only surface coil with active detuning between the transmit and receive coils. The mice were fixed in a supine position with the kidney area located directly over the surface coil. Single-voxel ^{1}H spectra from volumes encompassing most of one of the animal's kidneys were acquired before, during and after termination of the ~1-h BPA-F infusion, with a temporal resolution of 6.4 min per spectrum. The pulse sequence for these spectra was based on the LASER sequence (*25*), modified for BPA detection by the inclusion of a chemical-shift-selective excitation pulse focused on the aromatic proton peaks. The inter-echo delay was 4.6 ms, and the echo time (TE) was 27.6 ms. Typically, 256 scans were averaged with a repetition delay (TR) of 1.5 s. Before the BPA injection was started, one of the spectra was acquired without water suppression (using a single scan) and with the selective excitation centered on the water peak, providing a reference for the calibration of the BPA peak intensities. The calculation of absolute BPA concentrations was based on the intensity ratios measured for a phantom under the same circumstances (*24*). Multivoxel SI data were acquired with a double-echo pulse sequence (TE = 12 ms), using a chemical-shift-selective excitation pulse (focused on the BPA resonance) and two adiabatic slice-selective refocusing pulses, typically with 32×32 phase encode steps, TR = 1 s, for a total scan time of 17 min. The spatial resolution [slice thickness and field of view (FOV)] varied between different experiments and is reported in the Results section. SI reference maps of water were obtained in the same manner but without water suppression and with the excitation focused on the water resonance. The data were processed by 3DFT (two spatial + one spectral dimension), followed by sensitivity-enhancing exponential apodization (corresponding to 2 Hz broadening) along the spectral dimension, and by phase, baseline and frequency adjustments. Concentration maps for BPA were calculated by dividing the BPA by the water images as described in ref. (*24*).

In vitro experiments. Rat blood and excised mouse tumor samples were measured on a vertical bore 9.4 T spectrometer (Avance DMX400 WB, Bruker, Ettlingen, Germany) operating at 400 MHz for protons and at 128 MHz for ^{11}B at ambient temperature (21–23°C). ^{1}H spectra were acquired using a dedicated probe and 8-mm NMR sample tubes and ^{11}B spectra using a boron-free multinuclear probe and 10-mm tubes. The ^{1}H experiments were completed within 3 h of withdrawal of the blood samples, while the ^{11}B experiments were completed within 24 h of withdrawal of the blood samples, or killing of the tumor-bearing mice. All samples were at room temperature until their spectra were measured. Boron levels in the samples were calculated from the signal integrals relative to reference solutions with known concentration, taking into account the dilution factors.

RESULTS

Uptake and Washout Kinetics in Mouse Kidneys by Single-Voxel MRS

Representative results (Mouse A) illustrating how ^{1}H MRS can be used to follow the uptake kinetics of BPA *in vivo* are shown in Fig. 1. Panel A shows the location of the selected voxel on the anatomical MR image of a mouse kidney, and panel B shows three of the spectra, acquired (each during 6.4 min) from this voxel at the indicated times

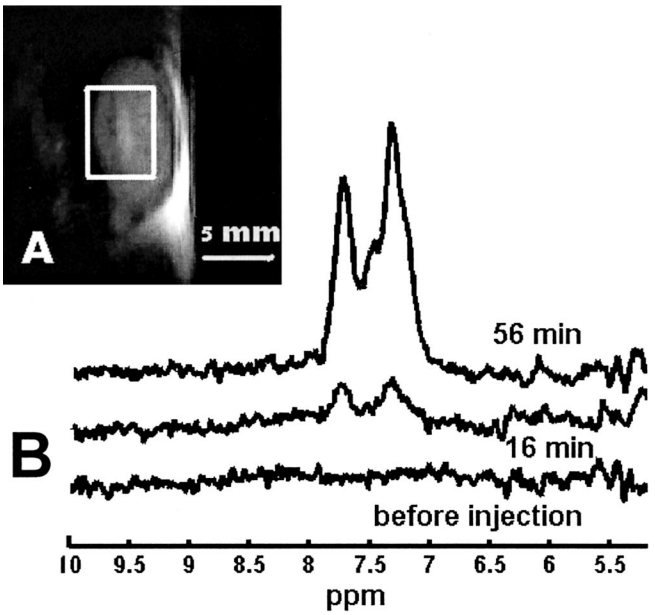

FIG. 1. Panel A: T_2-weighted MR image of Mouse A kidney with the voxel for LASER MRS superimposed. The voxel dimensions were 7 × 5.2 (in plane) × 4 mm. Panel B: Representative spectra from the selected voxel at the indicated times after the beginning of BPA-F injection. The spectra were processed with an exponential 2 Hz broadening sensitivity enhancement filter.

after the start of the BPA-F infusion. The peaks (growing with increasing time) represent aromatic protons in both the BPA-F complex and free BPA. The area under the peaks was used to calculate the corresponding total BPA concentration (complex + free), which was 11 m*M* (per volume of water) for the 16-min spectra and 82 m*M* for the 56-min spectra. The time courses of the total BPA concentrations for this experiment and for another similar experiment on Mouse B are shown in Fig. 2. At the end of the experiments, it was noticed that only Mouse A (represented by the circular data points) had urinated during the study, which could explain the different kinetics of clearance from the kidney in the two mice.

The upper spectrum in Fig. 3 was localized from the kidney of Mouse A 65 min after the start of the BPA-F infusion. The signal intensity corresponds to a total BPA concentration of 67 m*M*. The lower spectrum was localized from a phantom filled with a 6.5 m*M* total BPA solution, diluted from the injection solution. In this control spectrum, the improved spectral resolution allows the distinction between the peaks from free BPA (f) and the BPA-F complex (c), indicating that most of the BPA is in the fructose complex, as expected. However, comparing the *in vivo* spectrum to that of the phantom indicates that in the former most of the BPA was in the free form. This finding was corroborated in other experiments (see below).

Imaging of BPA in Mouse Kidneys by Spectroscopic Imaging (SI)

SI scans were accomplished in 17 min (see the Materials and Methods) before and after the start of the BPA-F infusion. Figure 4 shows results for Mouse B. Panel A shows the SI map for water, for which the scan was started 85 min after the start (and 23 min after the end) of the BPA infusion. The SI scans for this mouse were run with a slice thickness of 5 mm and a field of view of 6 cm, i.e., an in-plane resolution of 1.88 mm. The right-to-left signal intensity gradient is due to the sensitivity profile of the receiver surface coil located below (to the right in the image) the kidney. Panel B shows the BPA image, for which the scan was started 102 min after the start, or 40 min after the end of the infusion. Panel C shows the BPA spectroscopic image overlaid on the conventional MRI of the kidney region,

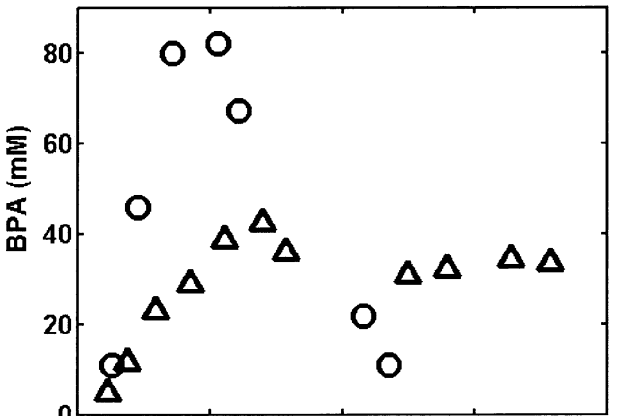

FIG. 2. Time-dependent concentrations of total BPA derived from the MRS results for two mice. The circles represent Mouse A, for which the injection lasted 50 min, and the triangles are for Mouse B, for which the injection lasted 62 min. The BPA signal was measured from a similar-sized voxel (0.14 ml).

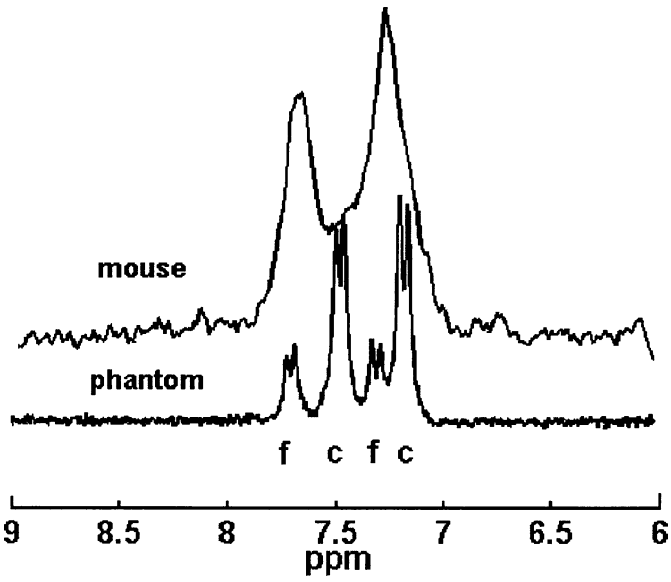

FIG. 3. Lower trace: The LASER spectrum of a 9 × 9 × 12-mm voxel from a phantom containing 6.5 m*M* total BPA, acquired with 256 scans, repetition time 1 s. Upper trace: Spectrum of Mouse A kidney obtained 65 min after BPA injection.

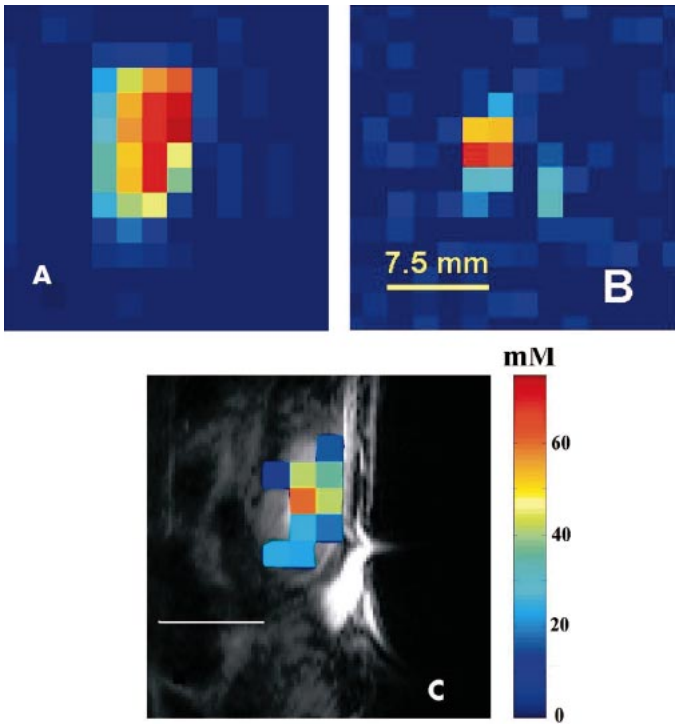

FIG. 4. SI metabolite maps for water (panel A) and total BPA (panel B) from a mouse kidney. Panel C: shows the calculated total BPA concentration map, overlaid on a T_2-weighted conventional MR image. The scale bar is 7.5 mm.

with the spectral intensities converted to total BPA concentrations, as described in ref. (*24*). The SI results for mouse A are shown in Fig. 5. Panel A shows the BPA concentration image overlaid on the conventional MR image. This scan was started 68 min after the start (18 min after the end) of the BPA infusion In this experiment, the slice thickness was 4.55 mm, and the in-plane resolution 1.4 mm; i.e., the voxel volume was 9 μl. The spectrum from a single 9-μl voxel in the center of the kidney is shown in the lower trace (Fig. 5B). The spectral resolution from such a small volume is much better than in the single-voxel MRS results shown in Fig. 1B, but is not good enough to clearly separate the peaks from BPA-F and free BPA, as in the spectrum from the phantom (Fig. 3). Therefore, the spectrum expected for a mixture of free BPA and the BPA-F complex was simulated; the result of this simulation is shown as the dot-dashed curve superimposed on the experimental spectrum in Fig. 5B. For the simulation, the aromatic protons in each molecular form were approximated as a weakly coupled AX spin system, with a scalar coupling constant of 7.8 Hz. The simulated spectrum was calculated assuming that 80% of the total BPA is free and only 20% is in the BPA-F complex, and its good agreement with the experimental spectrum confirms that most of the injected BPA-F complex was converted to free BPA. The chemical shifts for the complex were set to 7.20 ppm and 7.53 ppm and for the free BPA to 7.32 ppm and 7.74 ppm, and the peaks were convoluted with a Lorentzian broadening of 13 Hz. The upper spectrum in Fig. 5B was obtained by summing the spectra of 12 voxels covering most of the kidney. The signal-to-noise ratio is improved by this averaging, and the spectral resolution is almost equivalent to that in the lower spectrum due to correction of the field shift in each voxel (*24*).

Blood: BPA Clearance and Metabolism

The upper spectrum in Fig. 6 was obtained from the injected solution and shows, as expected, the dominance of the BPA-F complex compared to free BPA. Since these spectra were acquired at a 9.4 T field, the separation between the peaks is much clearer than at 4.7 T. The other spectra were obtained from the blood samples collected at the indicated times after injection. The spectral shift of the free BPA peaks is due to the lower pH in the blood compared to the injected solution. It is very clear that, as time progresses, more of the complex dissociates, and 20 min after the injection, most of the BPA is in free form, and the signal from the complex is barely detectable. Figure 7 shows a ^{11}B NMR spectrum of the 20-min sample, which also confirms the prevalence of free BPA. (The relative concentrations are proportional to the area of the peaks, not their height.) This ^{11}B spectrum does not show the presence of free borate, which could form as a result of hydrolysis of BPA. The clearance of boron from blood based on these spectra is shown in Fig. 8, where the curves represent free BPA and free BPA + complex (total boron).

Tumors

The ^{11}B NMR spectra of two tumor samples are shown in Fig. 9. Spectrum (a) was obtained from the tumor on Mouse I and spectrum (b) from the tumor on Mouse II. Mouse I was killed 18 min after injection, and the wet weight of the excised tumor was 0.55 g; Mouse II was killed 42 min after injection, and the wet weight of its tumor was 2.0 g. The tumor boron concentrations derived from these spectra corresponded to 17 μg/g for Mouse I and 55 μg/g for Mouse II. Similar to results obtained for blood and kidney, most of the BPA was in the free form and not in the complex from. Perhaps counterintuitively, the dissociation of the complex has progressed much more in the mouse with the shorter BPA circulation time (spectrum a), but the tumors on both mice were also different in size and composition. In both tumors, there is evidence for formation of free borate (B_i) (*26*), which was absent in the rat blood samples.

Extrapolation of Performance

For NMR, spatial resolution and sensitivity are directly related, since sensitivity is proportional to the number of nuclei detected, which in turn is proportional to the volume detected. Therefore, the linear dimension of the smallest resolvable volume element has an inverse cubic dependence on the minimal detectable concentration. Figure 10

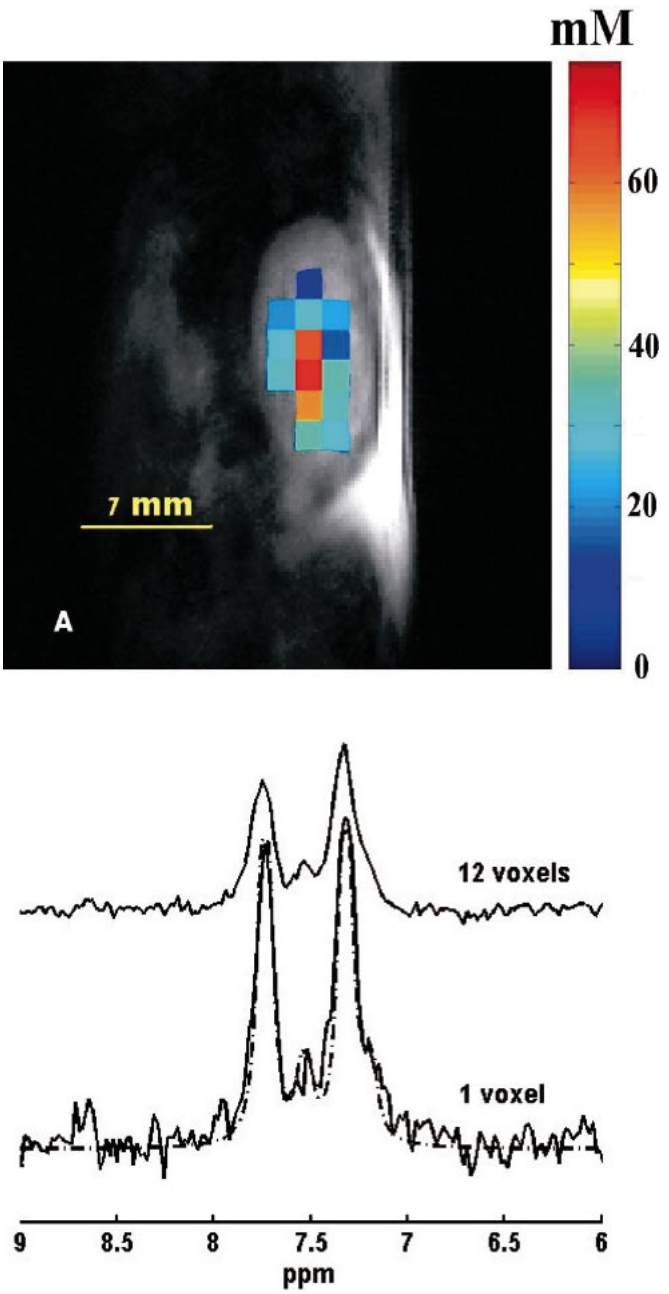

FIG. 5. Panel A: BPA concentration map overlaid on T_2-weighted MRI of mouse kidney. Panel B: lower spectrum: obtained from a single voxel in the center of the kidney, for which the calculated concentration was 0.07 *M*. The dashed curve is a simulated spectrum (see text). Upper spectrum: Obtained from summing the spectra of 12 voxels from the kidney.

shows graphs that correlate the minimal detectable boron concentration (in ppm) and the linear spatial resolution, based on a minimal SNR of 3:1 for detection. The curve labeled ''4.7 T, mouse'' was derived directly from the results of this study achieved for the chemical-shift-selective LASER spectra, with the scan time extended from 6.4 min to 15 min (the SNR increases proportional to the square root of the scan time). The other curves were calculated for patients based on the present results but corrected for conditions that will likely prevail for clinical MRS studies. First, the magnetic field for clinical scanners is generally 1.5 T or 3 T, which reduces the performance, since the SNR is approximately proportional to the field strength. Second, the RF coil for human experiments will be larger than for mouse experiments, which will also degrade performance. (The calculations in Fig. 10 assumed a fourfold reduction in SNR to account for this factor.) Since therapeutic boron levels are considered to be of the order of 20 μg/g boron, and tumor levels in patients could be as high as 40 μg/g (*5*), the performance predicted in Fig. 10 is encouraging.

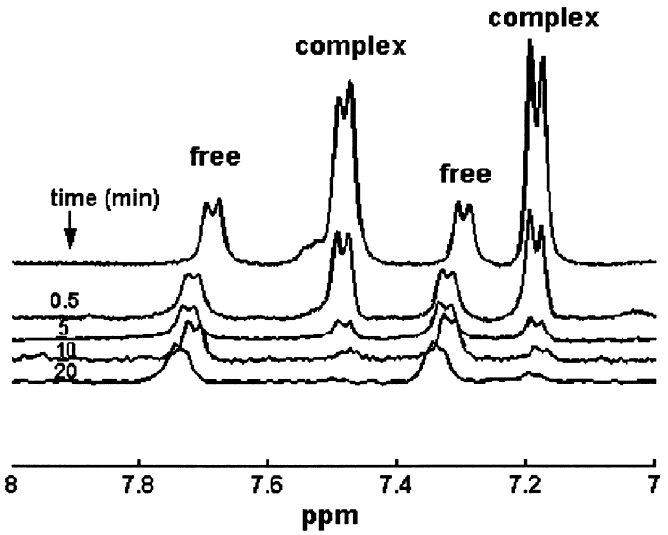

FIG. 6. ^{1}H NMR spectra, (9.4 T, 400 MHz, 16 averaged scans) of rat blood samples collected at different times after injection. The upper spectrum is from the injected solution.

DISCUSSION

At present, there is no practical method for measuring the distribution of BPA-F or BPA in patients undergoing

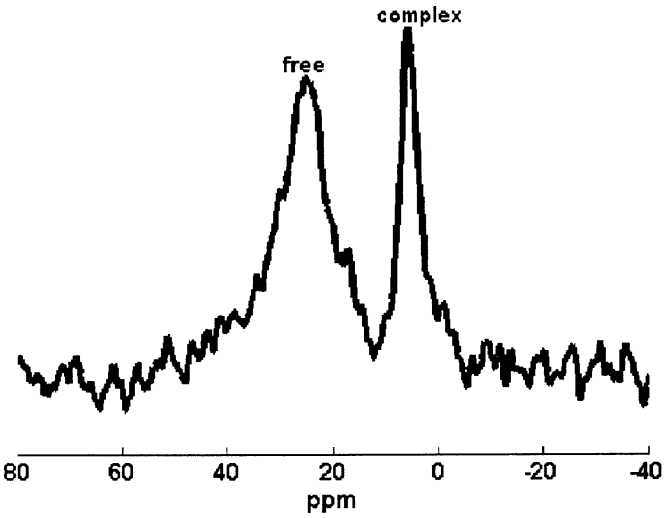

FIG. 7. ^{11}B NMR spectrum (9.4 T, 128 MHz, 12,000 scans acquired in 9 min) of blood sample collected after 20 min and processed with LB = 100 Hz exponential filter.

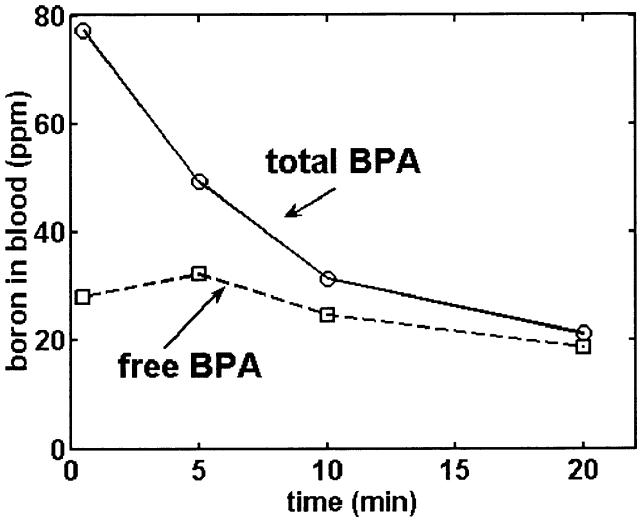

FIG. 8. Time course of boron concentrations in blood derived from the ^{1}H blood spectra for total BPA and free BPA.

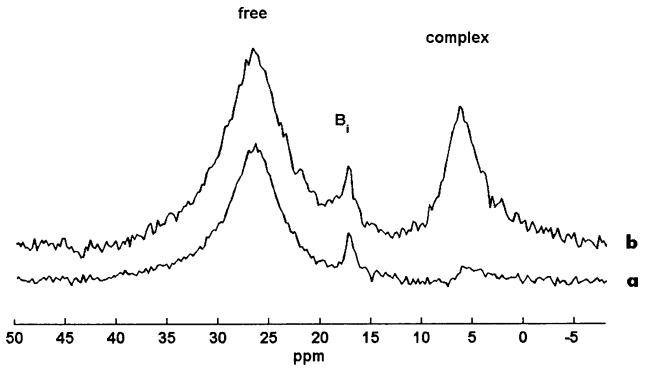

FIG. 9. ^{11}B NMR spectra (9.4 T, 128 MHz) of excised B33 tumor samples from two mice processed with LB = 15 Hz exponential filter. Spectrum (a) representing Mouse I was acquired in 5 h (400,000 scans), and the signal integral corresponds to a 17-μg/g boron concentration in the tumor. Spectrum (b) from Mouse II was acquired with 80,000 scans in 1 h, and the tumor boron concentration calculated from the tumor was 55 μg/g.

BNCT treatment. An ideal treatment protocol should include the possibility to conduct such measurements throughout and after termination of the drug infusion so that the optimal time for neutron irradiation as well as the boron-dependent radiation dose can be determined for each patient individually. A procedure currently applied involves the pretreatment administration and PET detection of ^{18}F-BPA (*9–11*), based on the assumption that the results of such studies correctly predict the uptake characteristics of BPA during the actual treatment infusion in the same patient. However, this ''rehearsal'' infusion is different from the actual BPA administration during treatment in two important aspects: First, the uptake characteristics of BPA could be different from those of its fluorinated analog, although recent results suggest that the cellular uptake may be similar, at least for cultured malignant cells (*27*). Second, the concentrations of the administered compounds used for the PET study are orders of magnitude smaller than those used for the radiation treatment, which could have a significant effect on the kinetics and on the partition between blood, tumor and surrounding tissue. Localized ^{1}H MRS and MRSI have the potential ability to detect BPA noninvasively during the actual preirradiation infusion of the material. To turn this possibility into a clinical reality that could significantly enhance the efficacy and safety of BPA-based BNCT, it is important to optimize the detection methods and maximize their performance. In this study, two experimental methods previously validated in phantoms (*24*), detecting and imaging BPA in the kidney were applied to live mice. The two techniques, chemical-shift-selective LASER and chemical-shift-selective SI, were found to be well suited for the quantitative detection of the aromatic ring protons in BPA, providing the spectral quality necessary for automated quantification procedures while minimizing signal intensity losses due to relaxation and the scalar coupling between the aromatic protons.

Extrapolation of the *in vivo* performance demonstrated here to examination of patients in clinical scanners predicts the possibility to map concentrations of $\geq\sim$20 μg/g boron with about 1 cm spatial resolution. Since the proposed methods target ^{1}H rather than ^{10}B, they can be implemented on standard clinical MRI scanners without the need for unusual hardware additions or modifications. Combining such MRS measurements with boron level measurements in the patients' blood samples could provide a realistic online measurement of tumor/blood ratios and radiation levels in the tumor. On the other hand, BPA concentration levels in normal brain could well be below the NMR detection level, so the radiation dose to normal brain tissue would still be uncertain. In any case, both MRI/MRS and PET cannot provide direct information about boron targeting characteristics at the cellular level, which is possible by techniques such as SIMS (*28*).

The results presented here showed that at higher mag-

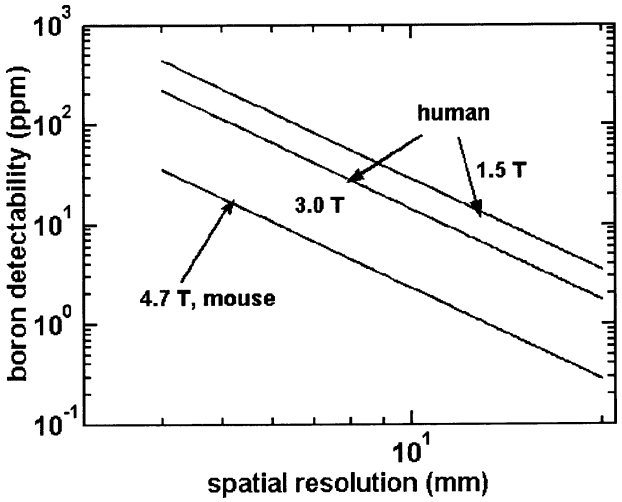

FIG. 10. Expected sensitivity/resolution performance curves for BPA detection under various experimental conditions.

netic fields (≥3 T), it is possible to distinguish between the signals from the free BPA and BPA-F complex molecules. The results showed that BPA-F, which is usually administered due to its superior aqueous solubility, rapidly becomes dissociated *in vivo*, and free BPA remains as the dominant molecular species. Previous evidence suggesting this behavior was observed in a study in which ^{19}F NMR spectroscopy was applied to detect ^{19}F-BPA-fructose in mice (*29*). In the present work, we also found evidence that BPA partially dissociated and that relatively minor amounts of inorganic borate were released in tumors. This was not seen in the blood of tumor-free rats. Similar findings were reported previously for cultured melanoma cells (*26*) as well as for blood samples from melanoma patients (*30*).

ACKNOWLEDGMENTS

This research was supported by the Israel Science Foundation founded by the Israel Academy of Sciences and Humanities. YS is the incumbent of the Tillie and Charles Lubin Professorial Chair in Biochemical Endocrinology.

Received: January 21, 2005; accepted: June 6, 2005

REFERENCES

1. R. F. Barth, A critical assessment of boron neutron capture therapy: An overview. *J. Neuro-Oncol.* **62**, 1–5 (2003).
2. M. Thellier, A. Chevallier, I. His, M. C. Jarvis, M. A. Lovell, C. Ripoll, D. Robertson, W. Sauerwein and M-C. Verdus, Methodological developments for application to the study of physiological boron and to boron neutron capture therapy. *J. Trace Micropr. Techn.* **19**, 623–657 (2001).
3. T. U. Probst, Methods for boron analysis in boron neutron capture therapy (BNCT). A review. *Fresenius J. Anal. Chem.* **364**, 391–403 (1999).
4. C. R. Gibson, A. E. Staubus, R. F. Barth, W. L. Yang, A. K. Ferketich and M. M. Moeschberger, Pharmacokinetics of sodium borocaptate: A critical assessment of dosing paradigms for boron neutron capture therapy. *J. Neuro-Oncol.* **62**, 157–169 (2003).
5. J. A. Coderre, A. D. Chanana, D. D. Joel, E. H. Elowitz, P. L. Micca, M. M. Nawrocky, M. Chadha, J. O. Gebbers, M. Shady and D. N. Slatkin, Biodistribution of boronophenylalanine in patients with glioblastoma multiforme: Boron concentration correlates with tumor cellularity. *Radiat. Res.* **149**, 163–170 (1998).
6. W. S. Kiger, M. R. Palmer, K. J. Riley, R. G. Zamenhof and P. M. Busse, A pharmacokinetic model for the concentration of ^{10}B in blood after boronophenylalanine-fructose administration in humans. *Radiat. Res.* **155**, 611–618 (2001).
7. P. Ryynanen, A. Kangasmaki, P. Hiismaki, J. Coderre, A. Z. Diaz, M. Kallio, J. Laakso, M. Kulvik and S. Savolainen, Non-linear model for the kinetics of ^{10}B in blood after BPA-fructose complex infusion. *Phys. Med. Biol.* **47**, 737–745 (2002).
8. P. M. Ryynanen, M. Kortesniemi, J. A. Coderre, A. Z. Diaz, P. Hiismaki and S. E. Savolainen, Models for estimation of the ^{10}B concentration after BPA-fructose complex infusion in patients during epithermal neutron irradiation in BNCT. *Int. J. Radiat. Oncol. Biol. Phys.* **48**, 1145–1154 (2000).
9. Y. Imahori, S. Ueda, Y. Ohmori, T. Kusuki, K. Ono, R. Fujii and T. Ido, Fluorine-18 labeled fluoroboronophenylalanine PET in patients with glioma. *J. Nucl. Med.* **39**, 325–333 (1998).
10. T. L. Nichols, G. W. Kabalka, L. F. Miller, M. K. Khan and G. T. Smith, Improved treatment planning for boron neutron capture therapy for glioblastoma multiforme using fluorine-18 labeled boronophenylalanine and positron emission tomography. *Med. Phys.* **29**, 2351–2358 (2002).
11. G. W. Kabalka, T. L. Nichols, G. T. Smith, L. F. Miller, M. K. Khan and P. M. Busse, The use of positron emission tomography to develop boron neutron capture therapy treatment plans for metastatic malignant melanoma. *J. Neuro-Oncol.* **62**, 187–195 (2003).
12. R. Kreis, Quantitative localized ^{1}H MR spectroscopy for clinical use. *Progr. Nucl. Magn. Reson. Spectr.* **31**, 155–195 (1997).
13. J. R. Griffiths and J. D. Glickson, Monitoring pharmacokinetics of anticancer drugs: Non-invasive investigation using magnetic resonance spectroscopy. *Adv. Drug Deliv. Rev.* **41**, 75–89 (2000).
14. I. M. Burtscher and S. Holtas, Proton MR spectroscopy in clinical routine. *J. Magn. Reson. Imag.* **13**, 560–567 (2001).
15. R. A. Komoroski, Biomedical applications of ^{7}Li NMR. *NMR Biomed.* **18**, 67–73 (2005).
16. W. Wolf, C. A. Presant and V. Waluch, ^{19}F-MRS studies of fluorinated drugs in humans. *Adv. Drug Del. Rev.* **41**, 55–74 (2000).
17. Y. J. L. Kamm, A. Heerschap, E. J. van den Bergh and D. J. T. Wagener, ^{19}F-magnetic resonance spectroscopy in patients with liver metastases of colorectal cancer treated with 5-fluorouracil. *Anti-Cancer Drugs* **15**, 229–233 (2004).
18. G. S. Payne, D. J. Collins, P. Loynds, G. Mould, P. S. Murphy, A. S. K. Dzik-Jurasz, P. Kessar, N. Haque, M. Yamaguchi and M. Leach, Quantitative assessment of the hepatic pharmacokinetics of the antimicrobial sitafloxacin in humans using *in vivo* ^{19}F magnetic resonance spectroscopy. *Br. J. Clin. Pharmacol.* **59**, 244–248 (2005).
19. P. Bendel, N. Koudinova and Y. Salomon, *In vivo* imaging of the neutron capture therapy agent BSH in mice using ^{10}B MRI. *Magn. Reson. Med.* **46**, 13–17 (2001).
20. P. Bendel, Biomedical applications of ^{10}B and ^{11}B NMR. *NMR Biomed.* **18**, 74–82 (2005).
21. C. S. Zuo, P. V. Prasad, P. Busse, L. Tang and R. G. Zamenhof, Proton nuclear magnetic resonance measurement of *p*-boronophenylalanine (BPA): A therapeutic agent for boron neutron capture therapy. *Med. Phys.* **26**, 1230–1236 (1999).
22. S. Heikkinen, A. Kangasmäki, M. Timonen, L. Kankaanranta, A-M. Häkkinen, N. Lundbom, J. Vähätalo and S. Savolainen, ^{1}H MRS of a boron neutron capture therapy ^{10}B-carrier, L-*p*-boronophenylalanine-fructose complex, BPA-F: phantom studies at 1.5 and 3.0 T. *Phys. Med. Biol.* **48**, 1027–1039 (2003).
23. M. Timonen, A. Kangasmäki, S. Savolainen and S. Heikkinen, ^{1}H MRS phantom studies of BNCT ^{10}B-carrier, BPA-F using STEAM and PRESS MRS sequences: Detection limit and quantification. *Spectroscopy* **18**, 133–142 (2004).
24. P. Bendel, R. Margalit and Y. Salomon, Optimized ^{1}H MRS and MRSI methods for the *in-vivo* detection of borono-phenylalanine (BPA). *Magn. Reson. Med.* **53**, 1166–1171 (2005).
25. M. Garwood and L. DelaBarre, The return of the frequency sweep: Designing adiabatic pulses for contemporary NMR. *J. Magn. Reson.* **153**, 155–177 (2001).
26. V. Panov, Y. Salomon, G. W. Kabalka and P. Bendel, Uptake and washout of borocaptate sodium and borono-phenylalanine in cultured melanoma cells: A multi-nuclear NMR study. *Radiat. Res.* **154**, 104–112 (2000).
27. S. Chandra, G. W. Kabalka, D. R. Lorey, II, D. R. Smith and J. A. Coderre, Imaging of fluorine and boron from fluorinated boronophenylalanine in the same cell at organelle resolution by correlative ion microscopy and confocal laser scanning microscopy. *Clin. Cancer Res.* **8**, 2675–2683 (2002).
28. D. R. Smith, S. Chandra, R. F. Barth, W. Yang, D. D. Joel and J. A. Coderre, Quantitative imaging and microlocalization of boron-10 in brain tumors and infiltrating tumor cells by SIMS ion microscopy: Relevance to neutron capture therapy. *Cancer Res.* **61**, 8179–8187 (2001).
29. P. Bendel, J. Zilberstein, Y. Salomon, A. Frantz, N. K. Reddy and G. W. Kabalka, Quantitative *in vivo* NMR detection of BSH and ^{19}F-BPA in a mouse melanoma model. In *Advances in Neutron Capture Therapy*, Vol. II, *Chemistry and Biology* (B. Larsson, J. Crawford

and R. Weinreich, Eds.), pp. 632–639. Elsevier Science, Amsterdam, 1997.

30. K. Yoshino, R. Nakajima, A. Takaoka, Y. Mori, H. Kakihana, Y. Mishima and M. Ichihashi, Determination of released boric acid *in vivo* after *p*-boronophenylalanine administration into melanoma-bearing subjects. In *Advances in Neutron Capture Therapy*, Vol. II, *Chemistry and Biology* (B. Larsson, J. Crawford and R. Weinreich, Eds.), pp. 334–338. Elsevier Science, Amsterdam, 1997.